Astron. Astrophys. 322, 938–942 (1997)

ASTRONOMY AND ASTROPHYSICS

Explanation of ^{29}SiO, ^{30}SiO and high-v ^{28}SiO maser emission

E. González-Alfonso[1,2] **and J. Cernicharo**[2,3]

[1] Universidad de Alcalá de Henares, Departamento de Física, Campus Universitario, E-28871 Alcalá de Henares, Madrid, Spain
[2] Observatorio Astronómico Nacional (OAN), E-28800 Alcalá de Henares, Madrid, Spain
[3] CSIC, IEM, Dpto. Física Molecular, Serrano 123, E-28006 Madrid, Spain

Received 7 May 1996 / Accepted 2 December 1996

Abstract. We have developed a non–local radiative transfer code to study the effects of line overlaps between different molecular species on the emergent line intensities from interstellar and circumstellar clouds. The numerical method solves the transfer of radiation and the statistical equilibrium populations for the different molecules simultaneously, and allows a direct comparison between the intensities calculated when overlaps are included/ignored in the models. We have applied the code to explain the maser emission in the rotational lines of ^{29}SiO, ^{30}SiO and high-v ($v \geq 3$) ^{28}SiO observed toward oxygen–rich circumstellar envelopes. The model calculations show that the pumping mechanism for most of these lines is dominated by infrared line overlaps between ^{28}SiO, ^{29}SiO and ^{30}SiO.

Key words: masers – radiative transfer – stars: AGB – circumstellar matter – ISM: clouds; molecules

1. Introduction

Maser emission in the rotational lines of ^{29}SiO and ^{30}SiO shows a conspicuous behavior which cannot be explained on the basis of the "classical" pumping mechanisms, radiative or collisional, proposed to account for the ^{28}SiO $v = 1$ and $v = 2$ maser emission (e.g., Bujarrabal & Nguyen-Q-Rieu, 1981; Lockett & Elitzur, 1992). The main problem arises from the contrast observed in the emission of adjacent rotational lines ($J+1 \rightarrow J$ and $J \rightarrow J-1$ of the same v-state), as occurs in the case of the ^{29}SiO $v = 1$ J=4 $\rightarrow$3 maser and its neighboring lines (Cernicharo et al., 1991). Standard models also fail to explain the observed maser emission in the $v = 0$ J=1 $\rightarrow$0 and J=2 $\rightarrow$1 lines of ^{29}SiO and ^{30}SiO (Alcolea & Bujarrabal, 1992). Emission in the high-v ($v \geq 3$) ^{28}SiO rotational lines displays similar contrasts to that of ^{29}SiO and ^{30}SiO (Cernicharo et al., 1993).

Cernicharo et al. (1991) proposed that infrared line overlaps between the three stable isotopomers of SiO could be responsible for these asymmetries. In particular, they suggested that the emission in ^{29}SiO $v = 1$ J=4 $\rightarrow$3 and the lack of maser emission in $v = 1$ J=3 $\rightarrow$2 and J=5 $\rightarrow$4 could be caused by line overlaps between ^{29}SiO and ^{28}SiO. By using an escape probability approach they reproduced the observed anomaly, and proposed that the $v = 0$ J=1 $\rightarrow$0 line of ^{29}SiO could be inverted by an analogous process. Furthermore, Cernicharo et al. (1993) suggested that the anomalous behavior of the ^{28}SiO $v = 3$ and $v = 4$ masers could also be a consequence of infrared overlaps between the SiO isotopes.

Although the LVG approach is a good starting point to evaluate the effects of line overlaps, the nature of the problem is non-local and the results of Cernicharo et al. (1991) need the confirmation of more complex and refined models. In this *Letter* we present a radiative transfer code which treats line overlaps in a non–local way and computes the statistical equilibrium populations for various molecules simultaneously. The application of the code to the problem of SiO masers confirms that most maser lines of ^{29}SiO, ^{30}SiO and ^{28}SiO high-v states, can be explained by infrared line overlaps.

2. The numerical code

Fig. 1 shows a schematic representation of the model adopted for the source. With the assumption of spherical symmetry, the source is divided in spherical shells within which the statistical equilibrium populations are computed. Each shell has uniform physical conditions, but the macroscopic gas velocity is allowed to vary within each shell. With initial guesses for the populations $n_j(m)$ in each level j and shell m, the simulation of the radiation field allows to compute $N_i(m)$, the *shell-averaged* number of radiative absorptions in each molecular transition i and shell m, produced per second, per unit of volume and per unit of population in the lower state of that transition (e.g., Bernes, 1979). $N_i(m)$ is equivalent to $B_i^{lu} J_i(m)$, where B_i^{lu} is the absorption coefficient and $J_i(m)$ is the angle–averaged radiation density in the m-shell. Once $N_i(m)$ is computed, the statistical equilibrium equations are solved to obtain better estimates for $n_j(m)$, and the process is repeated until the level populations in every shell converge on a solution. Bernes (1979) and González-Alfonso & Cernicharo (1993) simulated the radiation in the cloud by

Send offprint requests to: E. González-Alfonso

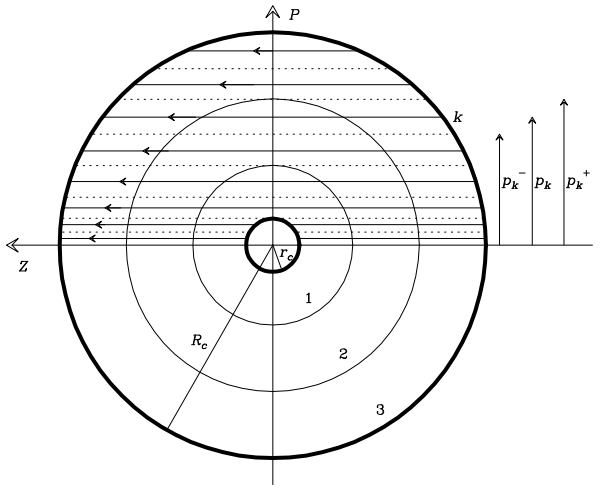

Fig. 1. Schematic representation of the model source. The spherical source, with radius R_c, is divided in a set of spherical shells, labelled $1, 2 \ldots$ The central source has radius r_c. The ray k is characterized by its impact parameter coordinate p_k, and represents the radiation traveling within coordinates p_k^- and p_k^+

means of model photons which represented all the real photons emitted in the source in one second. In the present method the radiation field in the source is simulated with "rays" which cross the source parallel to an arbitrary Z axis (Fig. 1). A large enough number of rays represents all the possible paths for the radiation in the source.

The discretization of the problem requires the division of the impact parameter P-axis in a set of intervals. The radiation field in the k-interval is simulated by a unique ray with p-coordinate p_k, and represents the radiation traveling within coordinates p_k^- and p_k^+. As usual, the frequency variable is also discretized in velocity intervals. With this aim the transitions are gathered in groups. Each group r contains all the transitions i_r, belonging to the same or to different molecules, which are blended. The r-group contains only one transition i_r if i_r is not overlapped with any other one. Each group r is divided in a set of velocity intervals of width δv; the intensity within each interval is considered uniform. The interval n has a velocity separation v_n relative to the central frequency ν_r of the group r. In this way the ray k represents at any position of its path the number of photons travelling in each interval n of each group r. At position (z, p_k), the ray k represents $W_k\, I_r^{n,k}(z)$ photons, where I denotes the radiation intensity at that position and the weight of the ray is $W_k = 4\pi^2[(p_k^+)^2 - (p_k^-)^2]\delta v/(hc)$.

At the beginning of its path in the cloud, the intensity of any k-ray for group r and interval n is $I_r^{n,k}(z_0) = B(\nu_r, T_{bg})$, where $z_0 = -\sqrt{R_c^2 - p_k^2}$, B is the Planck function and T_{bg} is the background radiation temperature. If the ray crosses the star, the emergent intensity from the stellar surface is $B(\nu_r, T_c)$, where T_c is the effective stellar temperature. Transfer of radiation along the rays is straightforward. Consider a k-ray entering the shell m at position z_{in}. For a given group r containing only one (non-overlapped) transition i_r, the intensity of the k-ray at the leaving point z_{out} of shell m is given by the familiar expression $I_r^{n,k}(z_{out}) = S_{i_r}^m + [I_r^{n,k}(z_{in}) - S_{i_r}^m]\exp\{-\tau_{i_r}^{n,k}(z_{in})\}$, where $S_{i_r}^m$ denotes the source function of transition i_r and $\tau_{i_r}^{n,k}(z_{in})$ is the opacity along the path between z_{in} and z_{out}. For groups r containing more than one transition S is no longer uniform within each shell, but depends on v_n and z. The path of the k-ray along shell m is divided in small segments within which the gas velocity component in the Z direction (v_z) is assumed to be uniform. Each segment length is chosen in such a way that the variation of v_z across it is smaller than δv. The variation of the intensity across a segment gives $I_r^{n,k}(z_{out}) = S_r^{m,n} + [I_r^{n,k}(z_{in}) - S_r^{m,n}]\exp\{-\tau_r^{n,k}(z_{in})\}$, where z_{in} and z_{out} now refer to the initial and final positions of the current segment, and $\tau_r^{n,k}(z_{in})$ is the sum of the opacities of the individual lines at velocity v_n. The source function is given by the sum of the emissivities divided by the sum of the absorption coefficients of the individual lines, and it does depend on v_n.

The number of radiative absorptions produced by the k-ray in transition i_r along its path or segment is

$$N_{i_r}^{n,k}\ (m) = \frac{W_k B_{i_r}^{lu} \tau_{i_r}^{n,k}}{V(m)[n_l(m)B_{i_r}^{lu} - n_u(m)B_{i_r}^{ul}]} \times \left\{ S_r^{m,n} + [I_r^{n,k}(z_{in}) - S_r^{m,n}] \frac{1 - \exp\{-\tau_r^{n,k}\}}{\tau_r^{n,k}} \right\} \quad (1)$$

where $V(m)$ is the volume of the m-shell, $B_{i_r}^{lu}$ and $B_{i_r}^{ul}$ are the coefficients of absorption and stimulated emission and n_l and n_u are the populations of the lower and upper levels of transition i_r, respectively. Equation (1) also applies for groups r containing only one transition i_r, substituting $S_r^{m,n}$ by $S_{i_r}^m$ and $\tau_r^{n,k}$ by $\tau_{i_r}^{n,k}$. The desired quantity, $N_{i_r}(m)$, is the summation of all $N_{i_r}^{n,k}(m)$ for every n, k and segment. When the level populations have converged, the main beam temperatures are calculated by using the same rays used in the simulation of the radiation field.

For SiO calculations, the code performs the following steps. First, it computes the equilibrium populations for the three molecules separately (^{28}SiO, ^{29}SiO and ^{30}SiO) by using the LVG approach. These populations are then used as initial values for the non-local calculation in which the line overlaps are still not considered. This second calculation is also done for each molecule separately, and is relatively quick due to the use of a completely diagonalized operator (see, e.g., Auer & Mihalas, 1969). We consider that the populations have converged when the maximum relative variation of any level population between consecutive iterations is lower than $c = 10^{-4}$, which is achieved in 5–10 iterations. Finally, these new level populations are used as initial values for the calculation which considers line overlaps. This calculation is done for the three molecules simultaneously, and uses exactly the same computational parameters (number of rays, velocity intervals...) as the preceding one. Hence, a direct comparison between the results of both non-local approaches gives the effect of line overlaps. The calculation with overlaps uses a normal Λ-iteration and a convergence criterion of $c = 10^{-3}$.

3. Models and results

The models solve the non-local radiative transfer for the populations of the 24 lower rotational levels in the 6 lowest v-states of ^{28}SiO, and of the 30 lower rotational levels in the 5 lowest v-states of ^{29}SiO and ^{30}SiO. The calculations ignore all the transitions $\Delta v \geq 3$ and all the overlaps amongst transitions with $\Delta v = 2$. The number of lines considered is 551 for ^{28}SiO and 552 for ^{29}SiO and ^{30}SiO. With the line widths and velocity gradients characteristics of our models (see below), only those overlaps with low frequency shifts are expected to have an important influence on the equilibrium level populations. From the preliminar results of Cernicharo et al. (1991), we have adopted only overlaps with velocity shift $\Delta V \leq 5$ km s^{-1}. The total number of groups is 77.

The physical conditions simulated in the models are the following: the central star has a radius of R_*= 5 10^{13} cm and an effective temperature of T_* = 2500 K (L_* = 1.8 10^4 L$_\odot$). The SiO molecules are located in a spherical region with internal and external radii of 1.4 and 3 R_*, respectively. This region is divided into 7 spherical shells with uniform physical conditions. The radial gas velocity varies slowly and linearly with radius, from 0.25 km s^{-1} to 0.5 km s^{-1} from shell 1 to shell 7. We also computed models with a large velocity gradient across the source (with a logarithmic velocity gradient ϵ between 3 and 5), and found results qualitatively similar to those presented below. The H_2 density, $n(H_2)$, is fixed to 3.5 10^{10} cm^{-3}. The ^{28}SiO abundance relative to H_2 is 5 10^{-5}, and the ^{29}SiO and ^{30}SiO abundances are 20 and 30 times lower respectively. The gas kinetic temperature is 1500 K, and the turbulence velocity (V_{tur}) is 1, 2 or 3 km s^{-1}. The collisional coefficients were taken from Bieniek & Green (1983). Dust grains are formed in more external layers of the envelope (r = 5 − 10 R_*), and their emission is neglected in our calculations. The above parameters simulate the physical conditions in the innermost regions of the circumstellar envelopes of oxygen-rich late-type stars (e.g., Bujarrabal, 1994); however, they are highly simplified. Quantitative results must therefore be considered as indicative.

Fig. 2 shows the resulting emergent line profiles of the most interesting SiO lines for the model with V_{tur} = 3 km s^{-1}. Intensities are given for a star located at a distance of D = 400 pc and observed with a telescope with HPBW= 15″. The insert boxes in some panels show the line profiles for the model with V_{tur} = 1 km s^{-1} (for other transitions the model results are qualitatively similar). Thin lines show the results when overlaps are not considered, and thick lines show the results obtained when they are included. We emphasize the high contrast obtained for some lines with and without overlaps. The overlaps can also reduce or completely remove the maser emission in some transitions (see the case of ^{28}SiO v = 3 J=2 →1). We will discuss now for each SiO isotopic species the maser transitions arising in our models that can be hardly explained with the standard models.

^{28}SiO: our models with low turbulent velocity can explain the maser emission in the v = 3 J=1 →0 line observed in a variety of sources (Scalise & Lépine, 1978; Alcolea et al., 1989). The maser is produced by the overlap between ^{28}SiO ($v = 4, J = 1$) → ($v = 3, J = 0$) and ^{28}SiO ($v = 1, J = 22$) → ($v = 0, J = 21$) ($\Delta V = -4.3$ km s^{-1}), and its strong dependence on the velocity dispersion is due to the effects of an additional overlap between ^{28}SiO $(2, 8) \rightarrow (1, 9)$ and $(3, 0) \rightarrow (2, 1)$. Our models explain the observed lack of maser emission in the ^{28}SiO v = 3 J=2 →1 line (e.g., Olofsson et al., 1985; Pardo et al., 1996), the maser v = 3 J=4 →3 detected in diverse sources (Cernicharo et al., 1993; Pardo et al., 1996) and the v = 4 J=5 →4 maser emission observed in VY CMa (Cernicharo et al., 1993). The lack of emission in the rotational transitions adjacent to those quoted above is also a natural effect of the pumping by IR overlaps. The maser v = 4 J=5 →4, with energy levels at ≈ 7 10^3 K, is produced in our models by the overlap between ^{29}SiO $(1, 28) \rightarrow (0, 29)$ and ^{28}SiO $(5, 3) \rightarrow (4, 4)$ (ΔV = 1.2 km s^{-1}). Our models also predict maser emission in the J=3 →2 rotational lines of the v = 3 and v = 4 states.

^{29}SiO: Strong maser emission in the v = 0 J=1 →0 line, which has been widely detected in evolved stars (e.g., Alcolea & Bujarrabal, 1992), is caused in our models by the overlap between ^{29}SiO $(1, 1) \rightarrow (0, 0)$ and ^{28}SiO $(2, 4) \rightarrow (1, 3)$ (−0.7 km s^{-1}). It also produces the maser in the v = 1 J=1 →0 line, which has been detected in TX Cam by Cho & Ukita (1995). The overlap between ^{28}SiO $(2, 5) \rightarrow (1, 4)$ and ^{29}SiO $(1, 2) \rightarrow (0, 1)$ (4.9 km s^{-1}) inverts the v = 0 J=2 →1 line at large V_{tur}. The relative intensities of these ^{29}SiO maser lines are very sensitive to the assumed value of V_{tur}. With low V_{tur} the v = 0 and v = 1 J=1 →0 line intensities increase, while the v = 0 J=2 →1 line weakens. Our models also reproduce the observed and already explained maser emission in the v = 1 J=4 →3 line (Cernicharo et al., 1991), whose intensity decreases with V_{tur}. The v = 2 J=2 →1 line, also masing in our models by the overlap between ^{29}SiO $(2, 2) \rightarrow (1, 3)$ and ^{28}SiO $(2, 7) \rightarrow (1, 8)$ (−4.9 km s^{-1}), has been detected in VY CMa (Cernicharo & Bujarrabal, 1992). Finally, the v = 2 J=4 →3 line of ^{29}SiO has been recently detected in four stars (González-Alfonso et al., 1997), and is produced by the overlap between ^{28}SiO $(3, 1) \rightarrow (2, 2)$ and ^{29}SiO $(2, 4) \rightarrow (1, 5)$ (2.3 km s^{-1}).

^{30}SiO: Strong maser emission is obtained in the v = 0 J=1 →0 line for low V_{tur}. The line has been detected in several stars (e.g., Barcia et al., 1989; Alcolea & Bujarrabal, 1992), and in our models is produced by the overlap between ^{30}SiO $(1, 1) \rightarrow (0, 0)$ and ^{29}SiO $(1, 3) \rightarrow (0, 4)$ (0.5 km s^{-1}). For $V_{tur} > 2$ km s^{-1} some competitive overlaps produce a reduction of the v = 0 J=1 →0 line intensity. These overlaps also induce the population inversion in the v = 1 J=2 →1 line; however, it has not been detected until present, although it has only been searched towards three stellar sources (Cernicharo & Bujarrabal, 1992; González-Alfonso et al., 1997). The overlap that causes the v = 0 J=1 →0 inversion also tends to favour the v = 1 J=1 →0 maser (which is already inverted with low amplification without overlaps), but two other overlaps between ^{30}SiO and ^{28}SiO destroy the population inversion in this line. Emission in the v = 1 and v = 2 J=4 →3 lines has been recently found by González-Alfonso et al. (1997) in several sources, and

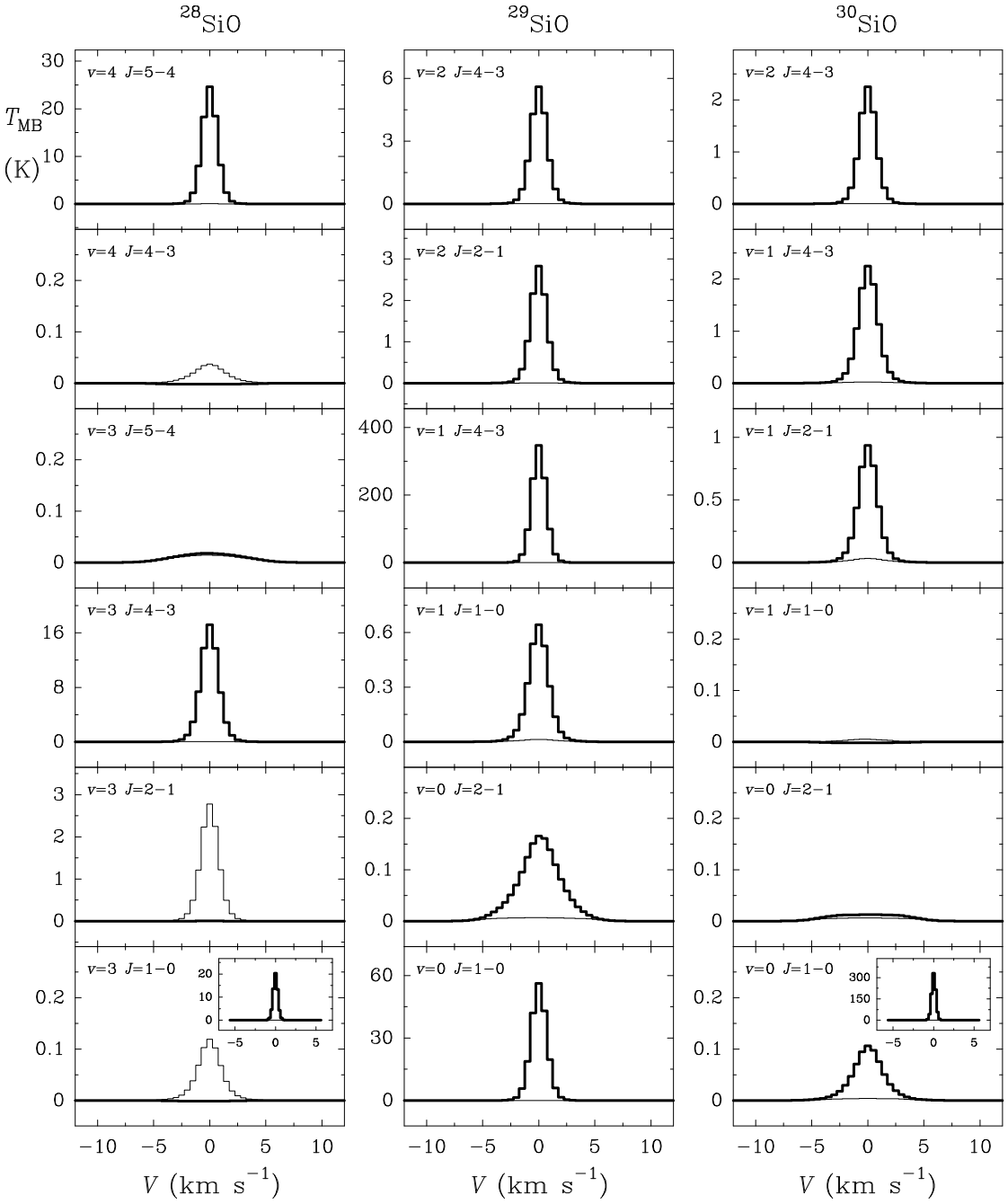

Fig. 2. Line profiles of various transitions for model with V_{tur} = 3 km s^{-1} computed when overlaps are taken into account (thick histograms) and when they are not (thin histograms). The star is located at 400 pc and the telescope HPBW is 15″ at every frequency. The insert boxes in some panels show the results for the model with V_{tur} = 1 km s^{-1}

such maser emission is also explained by infrared overlaps in our models.

We have also run some models with lower $n(H_2)$ (= 5 10^9 cm^{-3}) and T_* (= 2000 K). With these parameters, the intensities of most of the masers quoted above decrease to low and in some cases undetectable values –although the transitions remained inverted. There are, however, some transitions which do not follow this pattern: the intensity of the ^{29}SiO v = 0 J=2 →1 line increases, as is the case for the ^{29}SiO v = 1 J=3 →2 one (the later is not inverted in the models of fig. 2).

Although our models successfully explain most of the ^{29}SiO, ^{30}SiO and high–v ^{28}SiO maser lines detected so far (12 maser transitions), there are still some masers which are not reproduced. These are the v = 0 J=5 →4 and the v = 1 and v = 2 J=6 →5 lines of ^{29}SiO, and the v = 0 J=2 →1 and J=4 →3 lines of ^{30}SiO, which have been detected in several

sources (Cernicharo & Bujarrabal, 1992; González-Alfonso et al., 1997). These five maser transitions are also affected by IR overlaps, but in our models we do not obtain the inversion of the associated populations. We note that our limited set of models does not explore the full range of Doppler overlaps (those with $\Delta V > 5$ km s^{-1}) and of physical conditions in the star neighbourhood. Nevertheless, our models predict the presence of detectable maser emission from ^{29}SiO and ^{30}SiO transitions at submillimeter wavelengths. We have detected one of them, the ^{29}SiO $v = 3$ J=8 $\rightarrow$7 line ($\lambda \approx 0.9$ mm, $E \approx 5300$ K), in four circumstellar envelopes with the CSO telescope (González-Alfonso et al., 1996).

Acknowledgements. We thank P. Planesas and J. Alcolea for useful comments of the manuscript. This work has been partially supported by the Spanish DGICYT under grant PB90-408.

References

Alcolea J., Bujarrabal V., Gallego J.D., 1989, A&A, 211, 187
Alcolea J., Bujarrabal V., 1992, A&A, 253, 475
Auer L.H., Mihalas D., 1969, ApJ, 158, 641
Barcia A., Alcolea J., Bujarrabal V., 1989, A&A, 215, L9
Bernes C., 1979, A&A, 73, 67
Bieniek R.J., Green S., 1983, ApJ, 265, L29 (erratum: 270, L101)
Bujarrabal V., 1994, AA, 285, 953
Bujarrabal V., Nguyen-Q-Rieu, 1981, AA, 102, 65
Cernicharo J., Bujarrabal V., Lucas R., 1991, A&A, 249, L27
Cernicharo J., Bujarrabal V., 1992, ApJ, 401, L109
Cernicharo J., Bujarrabal V., Santarén J.L., 1993, ApJ, 407, L33
Cho S.H., Ukita N., 1995, PASJ, 47, L1
González-Alfonso E., Cernicharo J., 1993, A&A, 279, 506
González-Alfonso E., Alcolea J., Cernicharo J., 1996, AA, 313, L13
González-Alfonso E., Cernicharo J., Pardo J.R., 1997, in preparation
Lockett P., Elitzur M., 1992, ApJ, 399, 704
Olofsson H., Rydbeck O.E.H., Nyman L.A., 1985, A&A, 150, 169
Pardo J.R., Cernicharo J., Bujarrabal V., González-Alfonso E., 1996, submitted to A&A
Scalise E., Lépine J.R.D., 1978, A&A, 65, L7

This article was processed by the author using Springer-Verlag LaTeX A&A style file *L-AA* version 3.